JOURNAL OF GEOPHYSICAL RESEARCH, VOL. 100, NO. A9, PAGES 17,163–17,172, SEPTEMBER 1, 1995

Interplanetary magnetic field control of magnetotail field: IMP 8 data and MHD model compared

Zerefsan Kaymaz,[1] George Siscoe,[1] Janet G. Luhmann,[2] Joel A. Fedder,[3] and John G. Lyon[4]

Abstract. Magnetic field patterns in the magnetotail's cross-sectional plane at ~30 R_E derived from IMP 8 data are compared with corresponding patterns derived from the Fedder-Lyon MHD model of magnetosphere - solar wind interaction. The comparisons emphasize features attributable to the influence of the interplanetary magnetic field (IMF). They reveal considerable correspondences in field asymmetrics, nonuniform field perturbations, and current sheet twisting. Both data-based and MHD-based patterns are qualitatively similar to patterns obtained by superposing a uniform field on a dipole field, but they show that the field perturbations are stronger at the equatorial flanks of the tail than in the high-latitude lobes. These quantitative details go beyond the superposition model. From the point of view of interpretation, the fact that the MHD-based patterns reproduce the distinctive nonsuperposition features seen in the data-based patterns indicates that these features result from MHD motions within the magnetosphere distributing the field that is merged at the magnetopause (i.e., the "penetrating" field). From the point of view of modeling, the agreement indicates that MHD modeling captures essential aspects of the solar wind - magnetosphere coupling.

1. Introduction

The magnetotail response to the interplanetary magnetic field (IMF) holds key information on the nature of solar wind - magnetosphere coupling. To determine this response, we use IMP 8 measurements to map the magnetic field in a cross-sectional plane representative of 33 R_E [*Kaymaz et al.*, 1994a; *Kaymaz et al.*, 1994b, hereinafter referred to as Paper 1]. Paper 1 gives the average pattern of the tail magnetic field for various IMF conditions. Here we compare these patterns with corresponding patterns obtained with the Fedder-Lyon global MHD model [*Fedder et al.*, 1995; *Fedder and Lyon*, 1995].

In Paper 1, 5-minute ISEE 3 magnetic field averages are corrected for the transit time to IMP 8. The IMP 8 data are corrected for solar wind aberration and for neutral sheet warping according to *Fairfield*'s [1980] formula. The magnetic field vectors are binned for equatorial, northward, and southward IMF sectors defined by the field lying within 45° of the equatorial plane or within 45° of north or south respectively. For each sector the IMP 8 data averages are displayed on a rectangular grid of points spaced 2 R_E by 2 R_E. The average at each grid point includes all vectors in a column extending down the tail from 25 to 40 R_E and having a square cross section of 8 R_E on a side in the yz plane. The cross section is centered on the grid point.

The MHD simulations are based on numerical solutions of the ideal MHD equations which are used to model the solar wind interaction with the magnetosphere [*Fedder et al.*, 1995; *Fedder and Lyon*, 1995]. Reconnection occurs through numerical noise, though at a rate determined by boundary conditions, not by the magnitude of the noise [*Fedder and Lyon*, 1987]. We use the results for positive IMF B_y, northward IMF, and southward IMF. The negative IMF B_y case is considered to be the mirror of the positive IMF B_y case. In the model, the solar wind is steady with a density of 1.125 x 10^{-20} kg m^{-3} (n ~ 7 protons cm^{-3}), a velocity of 400 km s^{-1}, a Mach number (ratio of flow speed to phase speed of a fast mode MHD wave) of 10, and a magnetic field strength of 5 nT.

To make exactly commensurate comparisons with the IMP 8 data, cross-sectional maps of the MHD model magnetic field are prepared precisely as were the IMP 8 maps. Specifically, in the yz plane, the MHD model magnetic field data are interpolated to the IMP 8 field positions for each IMF sector, then smoothed in 8 R_E squares in the yz-plane. Because the model field changes little in the x range of the data, we take model values corrsponding to x = -30 R_E.

2. Comparisons

2.1. Equatorial IMF: IMF B_y

Paper 1 describes the asymmetries that an IMF B_y field induces in the magnetic field pattern in the cross-sectional plane of the tail. These asymmetries are described as departures from a symmetric dipolelike pattern representing the average of all IMF cases. The two poles of the dipole pattern are actually two-dimensional null points, that is, they are points where the y and z components of the field vanish. Topologically, the poles are nodes, that is, points of convergence or divergence. In the symmetrical reference pattern, these nodes lie in the midnight meridian, symmetrically about 8 R_E above and below the neutral

[1]Center for Space Research, Boston University, Boston, Massachusetts.
[2]Space Science Laboratory, University of California, Berkeley.
[3]Plasma Physics Division, Naval Research Laboratory, Washington, D.C., and SFA, Inc., Landover, Maryland.
[4]Department of Physics and Astronomy, Dartmouth College, Hanover, New Hampshire.

Paper number 95JA00593.
0148-0227/95/95JA-00593$05.00

sheet. B_y neutral sheet, we mean the line in the cross-sectional plane where B_x changes sign. We refer to the region between the two nodes and extending horizontally to both flanks as the internode region. It roughly corresponds to the plasma sheet, although the nodes lie outside the plasma sheet, and the plasma sheet's cross-sectional shape statistically resembles a bow tie more than a rectangle. We refer to the regions above and below the internode region as the north and south lobe regions, although again, the correspondence with the lobes is not exact.

Relative to the symmetrical reference pattern, the IMF B_y -induced asymmetries are the following: (1) the field lines in the internodal region skew in the direction of the IMF B_y, (2) the nodes shift in the y direction to follow the skew, and (3) the neutral sheet rotates in the direction opposite to skewing, and it does so nonuniformly (it is greater at the flanks than at the center).

Paper 1 quantitatively documents the nonuniform distribution of the IMF B_y -associated perturbation field in the cross-sectional plane. The perturbations are strongest on the flanks of the internode region and weakest in the center of the lobe regions. Further, the strong flank perturbations are stronger on one side of the neutral sheet than the other, and this north-south asymmetry is opposite on the two flanks.

Paper 1 notes that while the qualitative asymmetries cited above are consistent with simply superimposing a fraction of the IMF B_y field on the tail field, the nonuniform distribution of the perturbation amplitudes goes beyond such a superposition model. Part of the motivation for the present study is to determine how well an MHD model accounts for the distinctive nonuniform distribution of perturbation amplitudes. For this we compare these features with identically processed maps obtained using values generated by the MHD model of *Fedder et al.* [1995]. The qualitative and, when possible, quantitative comparisons made here include the asymmetries in the internodal region and lobe region fields, and the distribution of the perturbations.

2.1.1. Asymmetries in the internodal and lobe regions. We describe separately the skewing of the field pattern and the rotation of the neutral sheet.

2.1.1.1. Skewing of the fields and shifting of the nodes, data: Figures 1a and 1b show for the +IMF B_y case the IMP 8 magnetic field vector map and the "field line" map derived from it. The "field lines" are constructed in the yz plane (i.e., cross-sectional plane) using only y and z components of the field. They are not actual field lines nor projections of actual field lines. Their function is to reveal patterns. Hereinafter they will be called component lines to distinguish them from real field lines. Here the comparisons are made only for positive IMF B_y s. Negative IMF By patterns are the same after mirror reflection in the midnight meridian plane.

Figures 1a and 1b show the features of the symmetrical reference pattern described earlier and the IMF B_y -induced asymmetries in it. The field vectors converge and diverge from two topological nodes located about ±8 R_E away from the equatorial plane. The nodes separate the internodal region from the north and south lobe regions. The IMF B_y shifts the nodes about 2 R_E in the y direction, clockwise for positive IMF B_y. The component lines skew in the same sense. The skewing is more pronounced at the flanks of the internodal region than at the center.

Unlike internodal fields, lobe region fields show little asymmetry. Still, there are differences between their y and z components in the dawn and dusk lobes of both hemispheres. The y components are bigger in northern dawn and southern dusk regions; the z components are bigger in northern dusk and southern dawn regions.

2.1.1.2. Skewing of the fields and shifting of the nodes, model: Figures 1c and 1d show corresponding patterns compiled from a computer run of the Fedder-Lyon global MHD model for positive IMF B_y = 5 nT. Both model patterns are representations of a particular time. The magnetotail started its development to the condition seen in Figures 1c and 1d from a relaxed, northward IMF state. The patterns in the figures correspond to 2 h after the IMF turned to positive y direction. Still, the model magnetosphere is not yet completely developed; its features are still evolving.

Figures 1c and 1d exhibit the basic dipolar pattern with nodes, an internodal region, and lobe regions. In the internodal region the vectors tilt in the direction of the IMF B_y, more so toward the flanks, as observed in Figures 1a and 1b. The field magnitudes throughout the internodal region are seen to be comparable with those observed. The y direction shifts of the nodes are greater than observed, however, and less well defined. While the observed nodes are confined to a single grid point, the model nodes spread over several grid points in the y direction. If we take the least shifted nodelike grid point to represent the node, the shift is about 5 R_E in +y direction and about 8 R_E in the -y direction. The total shift, 13 R_E, is about 3 times bigger than observed. The model nodes are also found to be about 2 R_E farther from the equatorial plane than observed (10 R_E versus 8 R_E).

The component lines in Figure 1d spiral out of the southern node and into the northern node. Spiraling is not noticeable around the observed nodes. The presence of spiraling in the model and its absence in the data is the cause of the qualitatively different appearance between the observed and modeled lobes fields. The component lines over the nodes in the lobe regions are dominantly in the IMF B_y direction in the model and dominantly in the z direction in the data.

Detailed agreement between the observed and modeled fields should not be expected for the following reasons. The nodes' positions and the field strengths of the model magnetosphere are observed to change in time as the run progresses. As mentioned above, the magnetotail in Figures 1c and 1d is not fully developed; the tail field strength is increasing, particularly the B_x component, and the details of its structure are still changing. The model's patterns during the development depended on the initial conditions assumed for the IMF. For example, if the simulation had started from a southward IMF, the initial field strength would have been larger and the spatial position of the nodes would have been different. Thus the positions of the nodes are sensitive to the history of the IMF direction. The model patterns shown here preserve a memory of the initial northward IMF state. The data patterns, on the other hand, comprise a 4-year average of all IMF directions in the binning quadrant. Averaging tends to eliminate contingent details that depend on the history of

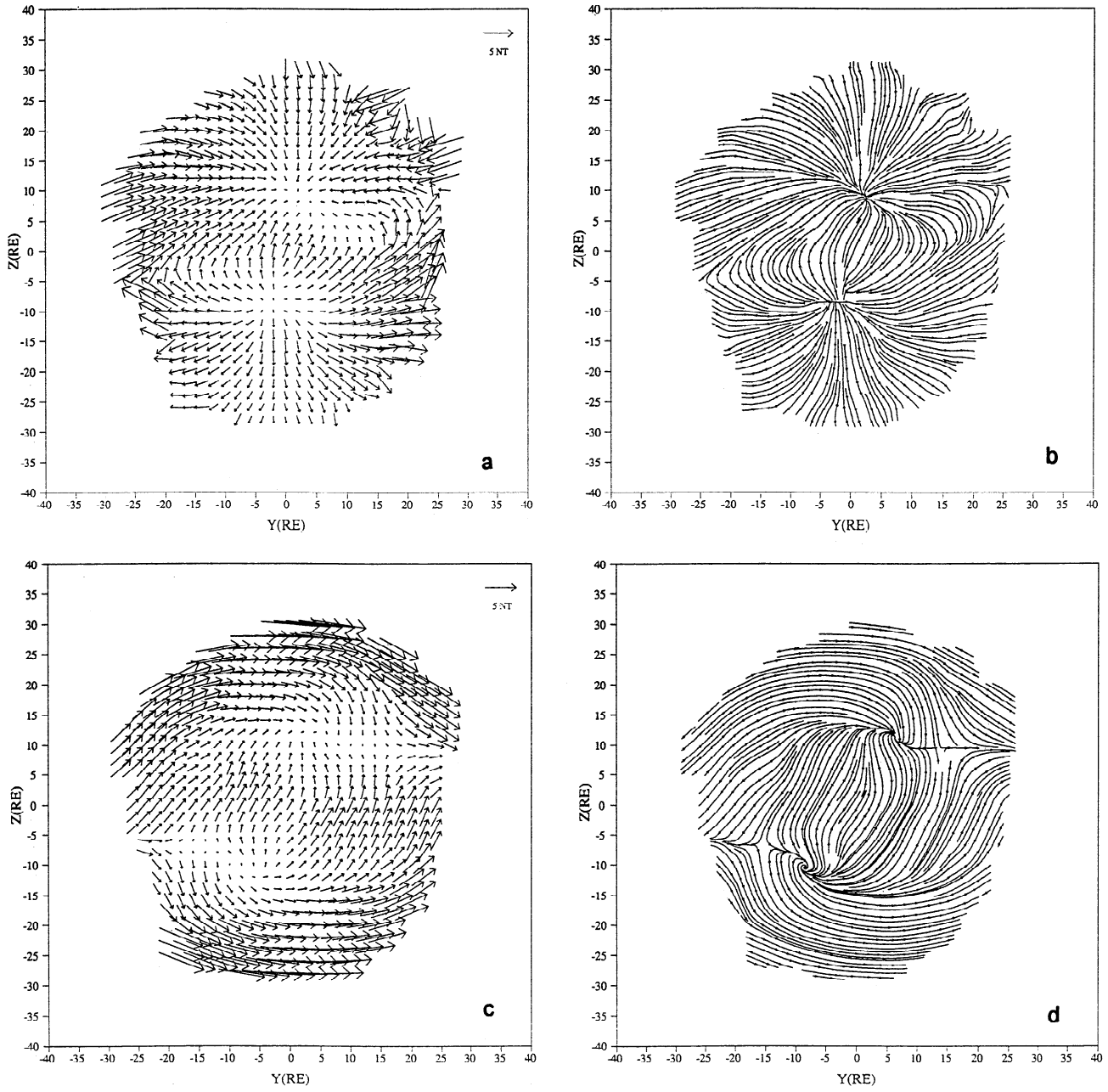

Figure 1. For equatorial IMFs, (a)IMP 8 magnetic field vectors and (b) magnetic component lines; (c) MHD magnetic field vectors and (d) component lines.

the IMF. More will be said on the spiraling of the model nodes later in the northward IMF comparisons relating to Figure 5.

Another contributor to the dissimilarity between the data and model patterns is the presence in the model pattern of a pair of diagonally matched saddle point singularities in addition to the nodes that correspond to the only singularities in data patterns. The model's quartet of singularities lies on two intersecting parabola-shaped separatrices, one concave to the left and one concave to the right.

In the data pattern, the model's saddle point singularities probably correspond to the apexes in Figures 1a and 1b of the closed component lines in the internodal region. These apexes occur at the boundary between the tail and the magnetosheath, the latter of which is a blank region in these figures. This suggests that the saddle points in Figures 1c and 1d might identify the tail boundary in the MHD model, which would be useful, since the boundary between the tail and the magnetosheath is difficult to specify in the model; it is not a sharp discontinuity but is spread out over several R_E. This spreading results in part from the limitations of the model and its finite spatial resolution. It results also in part from the 8 R_E averaging squares that were applied to prepare the patterns for comparison with the data. In averaging the data, magnetosheath observations were eliminated, whereas magnetosheath data were unavoidably included in the model

averages. The result is to blend magnetosheath and tail fields in the vicinity of the model boundary. This blending might contribute to making the model magnetopause as defined by the saddle points smaller than observed. Comparison with the unaveraged model pattern, however, shows that the effect is relatively small; the saddle points shift by an amount of the order of 1 R_E. The more important message is that the saddle point singularities appear to be real. In fact, they have been given a great emphasis by *Fedder et al.* [1995] (where they are called "topological points"). They also can be inferred in the IMP 8 data when the magnetosheath field is overlain on the tail data. A further discussion of saddle point singularities is reserved for a follow-up paper combining tail and magnetosheath IMP 8 data.

The model field vectors in the northern dawn and southern dusk lobes are dominantly y directed, whereas in the northern dusk and southern dawn lobes they are mainly z directed. This asymmetry agrees with the IMP 8 data shown here and with results reported by *Tsurutani et al.* [1984] at other tail distances. It is more pronounced in the model than in the observations. In general, the MHD model qualitatively reproduces the global IMF B_y effects seen in the IMP 8 data, but amplified and distorted.

2.1.1.3. Current sheet rotation, data: Figure 2 shows that the current sheet rotates counterclockwise in response to a positive IMF B_y. The line connecting the solid circles marks where the B_x component in the IMP 8 data changes sign, which is a standard operational definition for the current sheet. The rotation is nonuniform, being greater on the flanks and smaller, even reversed, in the center. The smooth solid line gives a cubic fit to the data. The average amount of rotation, found by a linear fit, is 8.3±1.7 deg.

2.1.1.4. Current sheet rotation, model: The line connecting the open triangles in Figure 2 marks the corresponding model current sheet. It shows a nonuniform, counterclockwise rotation similar to that seen in the observed average current sheet. There is also a suggestion in the model current sheet of a central reversal of rotation as seen in the data-based current sheet. The qualitative agreement between the cubic fits is unmistakable. Evidently, MHD modeling captures this distinctive feature of IMF-magnetotail coupling. The dashed line gives a cubic fit to the model results. The average rotation in the model current sheet is 11±0.9, which is somewhat larger than the average for the observed average current sheet, although the 1-sigma uncertainties in the two averages touch.

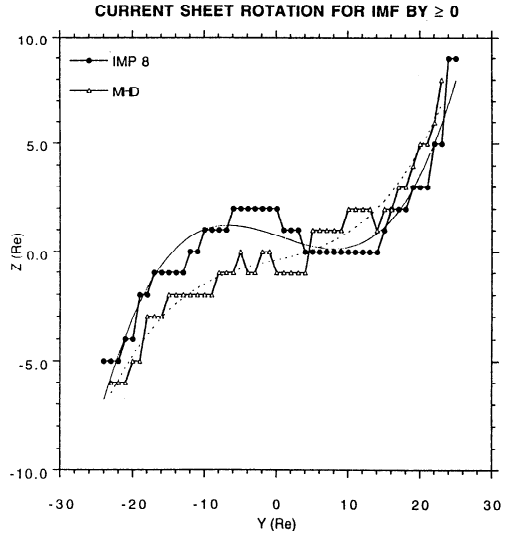

Figure 2. Current sheet, as determined from the B_x reversal points, rotation for positive IMF B_y. Solid circles connected with the thick line show the IMP 8 current sheet while the open triangles connected with the hin line show the MHD model current sheet. The smooth lines give cubic fits to the IMP 8 data (solid line) and the model results (dashed line).

2.1.2. Difference vectors. Subtracting the vectors in the negative IMF B_y vector map from the vectors in the positive IMF B_y vector map, as described in Paper 1, lets one isolate the IMF B_y-associated perturbation fields. This subtraction technique eliminates all sources of B_y and B_z that are not associated with the IMF, since these stay constant when IMF B_y changes sign and thus are eliminated in the subtraction. Paper 1 shows that the resulting perturbation vectors are strong in some parts of the tail cross section and weak in other parts. As described below, the places where the perturbation field is strong and weak form a distinctive pattern. As in the case of the nonuniform rotation of the current sheet described above, this pattern of nonuniform perturbation strengths offers a good test for the predictive powers of a quantitative tail model. Here we test how well the Fedder-Lyon global MHD model simulates the observed nonuniformity.

2.1.2.1. Distribution of the difference vectors over the tail cross section, data: Figure 3a shows the perturbation vectors obtained by subtracting the negative IMF B_y map (not shown here) from the positive IMF B_y map (Figure 1a). The vectors are predominantly in the +y direction (with some exceptions to be noted below in comparison with the model perturbations) but, as noted, their strengths vary greatly and systematically over the cross section. The pattern is ordered from left to right into strong dawn, weak central, and strong dusk sectors, but the lobe portion of each sector is weakest. Thus the strongest fields appear in the equatorial flanks, and the weakest fields appear in the central lobes. Quantitatively, relative to the concurrently measured IMF B_y, the strength of the perturbation field, determined by halving the difference vectors, is about 29% in the equatorial flanks while only about 9% in the lobes.

2.1.2.2. Distribution of the difference vectors over the Tail cross section, model: Exactly analogous to Figure 3a , Figure 3b gives the difference vectors for the model field. For this, the negative IMF B_y map was taken to be the mirror image of the positive IMF B_y map, Figure 1c. Since it is difficult to define the magnetopause location in the MHD model, we arbitrarily put it at a radius of 20 R_E.

Compared to the map of observed average perturbation vectors, the map of model perturbation vectors is in general more symmetrical, since by construction, the features appear identically in both hemispheres at mirror locations. Also, unlike the observed case, the strongest vectors occur near the northern and southern boundaries. These big difference vectors, however, almost certainly result from mixing magnetosheath vectors in with tail vectors in the averaging process. The magnetosheath vectors are strongest in these

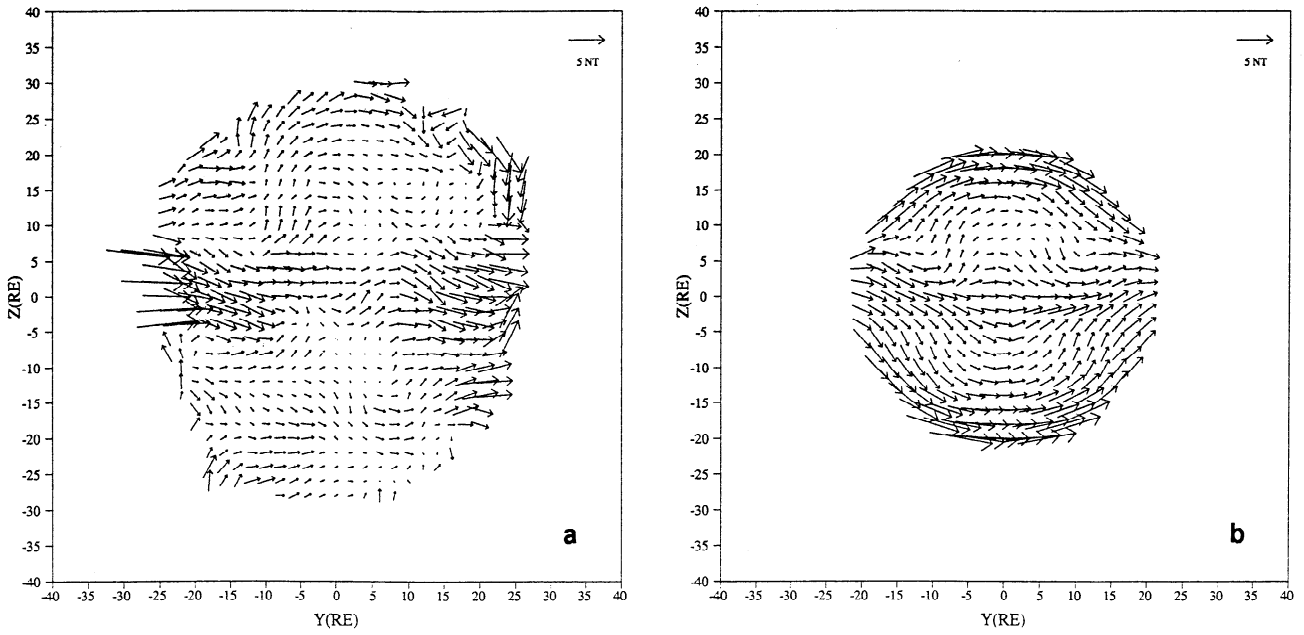

Figure 3. (a) IMP 8 magnetic field difference vectors. (b) Fedder and Lyon MHD model difference field vectors.

regions, and they add instead of cancel when the positive and negative vector maps are subtracted to find the perturbation field. Thus the model's big high-latitude perturbations are very likely artifacts of the averaging procedure.

More significant is the fact that, like the observed case, the model perturbations are stronger in the equatorial band than in the lobes. This result is insensitive to the mixing-in of magnetosheath fields by averaging, since the strong perturbations extend deeper into the tail than can be reached by averaging. Quantitatively, the strengths of the model perturbations are reasonably consistent with the observed perturbations across the equatorial band. There are two other interesting correspondences between the patterns in Figures 3a and 3b. The weaker, central portion of the equatorial band of strong perturbations in the data pattern is represented in the model pattern by a circular detour feature with a weak (actually reversed) central field. The other correspondence is a feature seen best in the model pattern. This is the large, circular track that begins and ends at the equatorial band of strong vectors and encloses the central lobe. There is one such track in each hemisphere. To make the track circular, the perturbation vectors are nearly straight north or south as they diverge from the equatorial band of strong perturbations. The feature is very distinct in the model pattern. It is less so in the data pattern, but a vestige of it seems nonetheless to be discernible, especially in the northern hemisphere. Here nearly the complete track can be traced; the northward leg is actually quite pronounced. Without the MHD simulation for comparison, however, it was not recognized in Paper 1 to be a possibly significant regularity.

In the lobes, the model seems also to capture the diagnostic features of the data with weaker central lobe perturbations and stronger dawn and dusk lobe perturbations. A similarity with the data is also evident with regard to the difference between the central lobe and central plasma sheet perturbations, with the central lobe perturbations being weaker. Although both the plasma sheet and the lobes show the nonuniform distribution of perturbations between the dawn, central, and dusk sectors, the differences are less than in the observed case. Finally, in both hemispheres there is a clear tendency for the strength of the model perturbations to increase from the central lobes to the central boundary. Not all this increase can be attributed to the mixing in of magnetosheath vectors in the averaging. This tendency is also present in the data patterns, since the weakest perturbations lie near the positions of the nodes in the original patterns, that is, near the border between the plasma sheet and the lobes.

2.1.2.3. Distribution of the difference vectors with respect to the current sheet, data: Figure 4a overlays the data-based twisted current sheet from Figure 2 on the data-based IMF B_y perturbation vector field of Figure 3a. The picture reveals a subtle, but probably significant, newly discovered asymmetry reported in Paper 1, viz., the strongest perturbations for this positive IMF B_y case lie above the current sheet on the dawnside and below it on the duskside. This combined dawn-dusk and north-south asymmetry between the current sheet and the perturbations suggests that the twisting of the current sheet and the localization of strong perturbations are two aspects of one process. Such a process might be dayside magnetic merging between the geomagnetic field and the IMF with a dominant y component and the consequent flow pattern within the magnetosphere. The question that can be addressed here is whether this process is a global MHD process, which should show up in a global MHD simulation.

2.1.2.4. Distribution of the difference vectors with respect to the current sheet, model: Figure 4b shows the model-based current sheet and perturbations overlain as in Figure 4a. The diagnostic asymmetry is indeed present. The largest of the strong equatorial flank perturbations lie above the current sheet on the dawnside

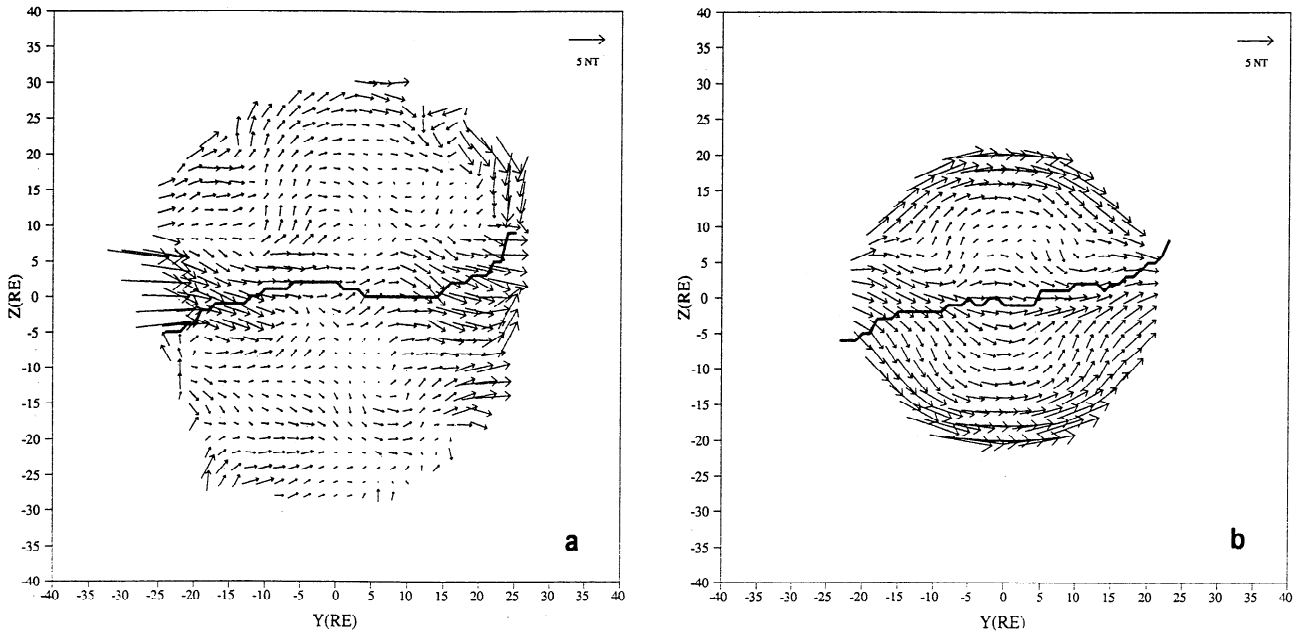

Figure 4. (a) Difference field vectors overlapped on the current sheet rotation for positive IMF B_y. (b) Same as Figure 4a but for MHD model results.

and below it on the duskside. The separation between the region of strongest perturbations and the current sheet is perhaps even clearer in the model pattern than in the data-based pattern. The presence of the asymmetry in the model pattern supports the idea that the same asymmetry seen in the data-based pattern is the result of a global MHD process.

2.2. Dominantly northward and southward IMFs

Paper 1 shows that the differences between the northward and southward IMF cases can be expressed in terms of the relative sizes and shapes of the domains of dipolar and flaring component lines. (Here "flaring" means nondipolar.) Briefly, for northward IMFs, dipolar component lines fill most of the tail's cross section, while for southward IMFs, flaring component lines fill most of the tail's cross section. Paper 1 also reports the following unexpected and significant finding bearing on reconnection models: The strongest perturbations associated with IMF B_Z lie along the flanks of the tail rather than down the center. This result extends to the southward IMF case the finding mentioned above for the equatorial IMF case, i.e., the strongest perturbations occur on the equatorial flanks, and the weakest perturbations occur in the lobes. The following compares these observed properties of IMF B_Z effects with the corresponding properties produced by the MHD model.

2.2.1. Magnetic Field Vectors. We consider separately the northward and southward IMF cases.

2.2.1.1. Northward IMF, data: Figures 5a and 5b, reproduced from Paper 1, show the magnetic field vectors and component lines for northward IMF. Compared to the asymmetric equatorial IMF patterns in Figures 1a and 1b, these patterns are reasonably bilaterally symmetric. Figure 5b shows dipolar component lines with circular shapes (or at least nonapical shapes in contrast to true dipolar lines) filling the cross section except at the poles. This pattern resembles the circularly enclosed dipole pattern that results from superimposing a uniform northward field on a two-dimensional dipolar field such as the symmetrical reference field described at the beginning (i.e., the average of all IMF cases). However, a uniform superposition model does not reproduce well the behavior of the field strength. The field strength in the internodal region, as Figure 5a shows, roughly doubles from the center of the tail to the flanks, which is a noticeably bigger increase than for the reference field [*Kaymaz et al.*, 1994a]. Also at high central latitudes, the field strength does not drop as if approaching the neutral points in a northward superposition model [e.g., *Cowley*, 1973]. Thus the global pattern in this case owes its distinctive, circular-dipole-dominated geometry to the influence of a nonuniform northward perturbation.

2.2.1.2. Northward IMF, model: Figures 5c and 5d give the corresponding patterns for the model field for a 5 nT northward IMF. They seem to capture the distinctive geometrical aspect of Figures 5a and 5b that distinguish them from the symmetrical reference field, and even to exaggerate the distinction. The equatorial field strength increases about a factor of 3 from the center to the flanks, which also is an exaggeration of the observed case.

The most conspicuous difference between the model and observed patterns, seen best in the component line map (Figure 5d), is that the model's nodes are stretched out, extending over several grid points and ending in pronounced spirals. The observed nodes for this northward IMF case (Figure 5b) are also somewhat stretched out but much less so by comparison, and there are no spirals. For the model the pattern might better be described as having two nodes separated by a saddle point singularity in each hemisphere. The stretching of the model's nodes over nearly 15 R_E turns the nodes into topological limit cycles or attractors in the parlance of nonlinear dynamics, lines toward which all neighboring lines converge asymptotically. The sense of the spirals at the tips of the cycles gives an algebraic sign

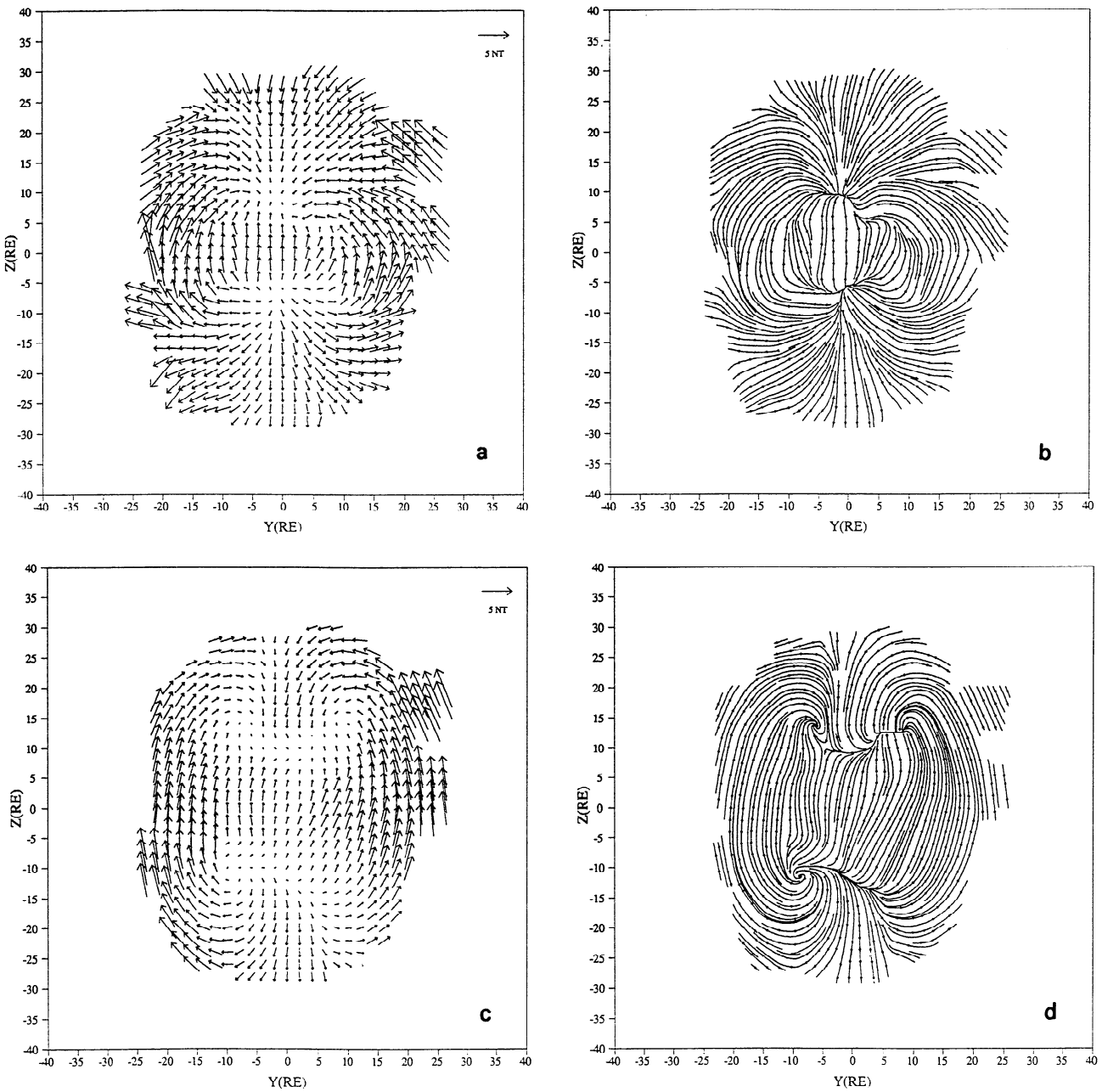

Figure 5. For northward IMF (a) IMP 8 magnetic field vectors and (b) magnetic component lines; (c) Fedder and Lyon MHD model field vectors and (d) component lines.

(e.g., plus or minus) to the nodes. The two dawnside nodes have the same sign, as do the two duskside nodes. Instead of "plus" or "minus," the sign of a node can be specified by the direction of the current needed to give a spiral of the observed sense: away from Earth on the dawnside and toward Earth on the duskside. This is consistent with the direction of the Birkeland currents present in the ionosphere during northward IMF B_z (NBZ currents). Therefore these model nodes are consistent with the polar convection cells in the four cell convection pattern that becomes established during northward IMF.

More fully stated, the degree and sense of spiraling of the model nodes depend on the strength of the currents and their direction toward or away from Earth. Their strength and direction as well as their position depend sensitively upon the direction of the IMF and its immediate history. The snapshots in Figures 5c and 5d were taken 5 magnetosphere hours into a run for which the IMF was held straight northward and constant at 5 nT. One result of holding conditions fixed and constant for so long is to produce well-developed, sharply defined limit cycles and spirals. That they are not well developed or sharply defined in the data-based maps is probably because these maps average over uncorrelated histories of the IMF that affect the values of individual vectors in the average. This is probably also the reason that the model nodes are farther apart than the data-based nodes.

The northward IMF model run with its symmetrical, well developed limit cycles and spiral nodes lets us understand better the features in the model run discussed earlier for positive IMF B_y shown in Figures 1c and 1d. If we start with the symmetrical northward IMF case and tilt the IMF

toward dusk (i.e., in the +y direction), the influence of the northern dawn node will grow at the expense of the influence of the northern dusk node. This progressive change takes the form of duskward migrations of the dawn node and the saddle point, while the dusk node becomes less distinct as a separate feature. The situation in the south lobe progresses with mirror symmetry. If the IMF continues to toward $+B_y$, the migration of the northern dawn spiral will continue until the northern dusk spiral disappears, leaving just the dawn spiral, which has now moved to the duskside. The saddle point is still visible duskward of the relocated dawn node.

2.2.1.3. Southward IMF, data: Figures 6a and 6b, reproduced from Paper 1, show the magnetic field vectors and component lines for southward IMF. Here too, as in the northward IMF case, the patterns are reasonably bilaterally symmetric compared to the equatorial IMF case. In contrast to the northward IMF case, however, the domain of dipolar component lines is confined to an equatorial band, above and below which extend the domains of flaring component lines. The angular sweep of the flaring component lines is about 180°, similar to that for the equatorial IMF case, but here there is no rotational twisting of the field line pattern. The basic geometry resembles the open pattern that results from superimposing a uniform southward field on a two-dimensional dipolar field. The flaring component lines correspond to the superposition's open component lines. The apexed (as distinct from circular) component lines in the internodal region suggest the presence of equatorial nulls, as also occur in the superposition model. As in the northward IMF case, however, the behavior of the field strength is not predicted by the superposition model. Figure 6a shows that in the internodal region, the field strength increases from the center of the tail to the flanks

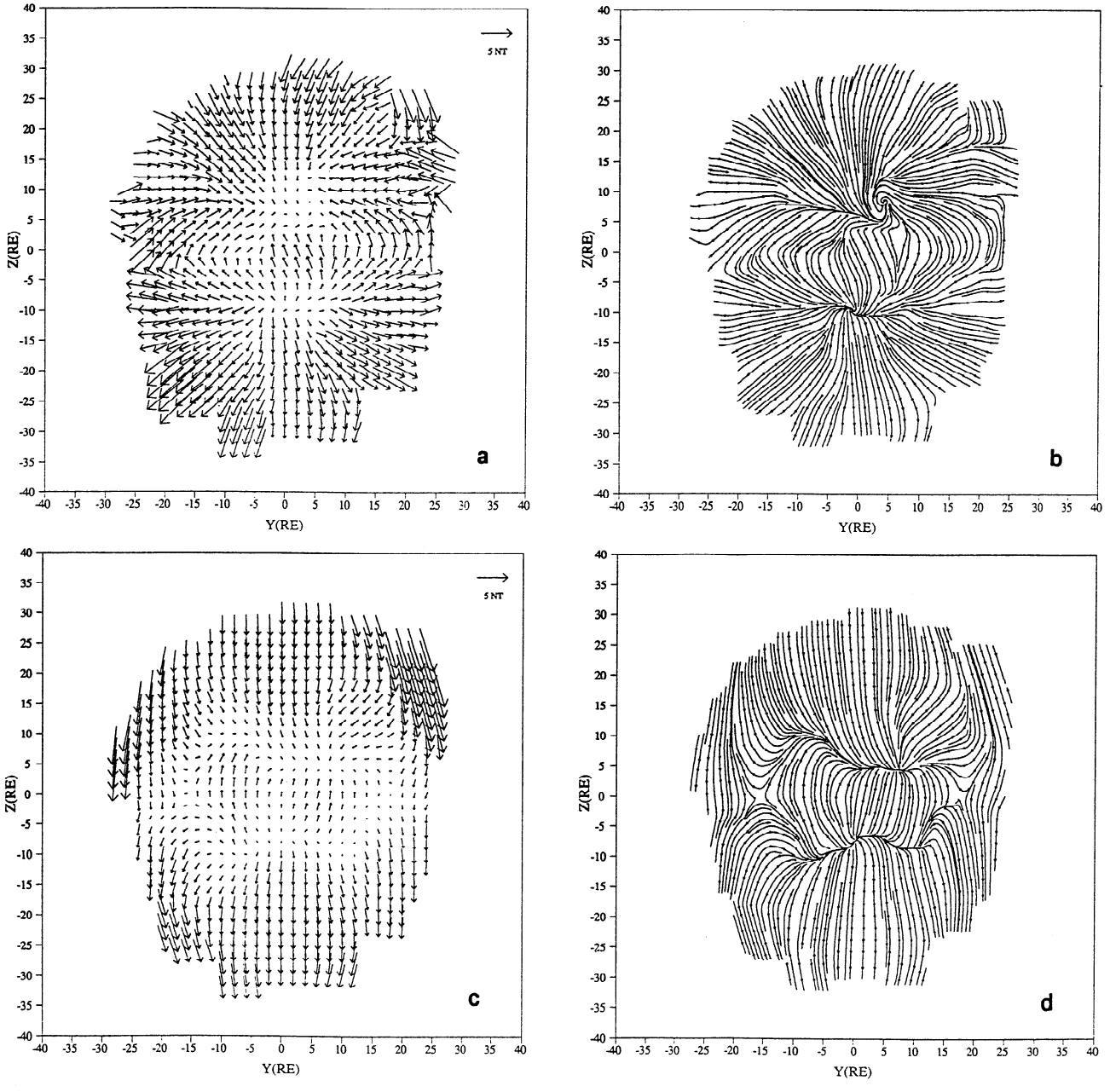

Figure 6. Same as Figure 5 but for southward IMFs.

but less so than in the northward IMF case. The conspicuous northern hemisphere spiral in Figure 6b with no southern counterpart indicates that not all features are stable components of the averages. Nonetheless, comparing the equatorial, northward, and southward IMF cases shows that the IMF distinctly individualizes all three.

2.2.1.4. Southward IMF, model: Figures 6c and 6d give the model vectors and the component lines for a 5 nT southward IMF. For this southward IMF snapshot, the model magnetosphere is toward the end of the substorm growth phase (approximately 5 minute before the expansion phase). The pattern they describe shares with Figures 6a and 6b the same distinctive characteristics relative to the equatorial and northward IMF patterns, that is, (relative) bilateral symmetry, a dominance of flaring component lines, and dipolar component lines confined to an equatorial band. As for the other cases, there are also differences between the data-based and model-based patterns. The model-based dipolar component lines are less apexed, which is associated with the fact that the model-based nodal lines (actually, topological limit cycles) are more stretched. Comparing field strengths shows that the model fields are generally smaller than the observed fields in both the internodal region and the lobes. Here again, the model magnetosphere for this configuration is still fairly early in a growth phase, and the tail lobes have not reached full strength. The equatorial nulls expected on the basis of the superposition analogy are actually present in the model-based pattern. These nulls in Figure 6c lie in regions of fairly strong B_y in Figure 6a. Still, the component line map in Figures 6b shows nascent nulls where Figure 6d shows actual nulls.

2.2.2. Difference vectors. Figure 7a shows the data-based perturbation field obtained by subtracting the northward IMF vectors (Figure 5a) from the southward IMF vectors (Figure 6a). Figure 7b shows the corresponding pattern for the model-based field. An important result, discussed in Paper 1 for the data-based pattern but seen here in both patterns, is that the strongest perturbations are concentrated on the flanks of the tail. The weakest perturbations define a broad strip running north-south down the center of the pattern. In the data-based pattern, the vertical, central strip of weak perturbations is more evident in terms of the z component of the field, which is the relevant component in this case.

Superposition models of the interconnection between the IMF and tail field would impose a uniform southward perturbation field over the tail cross section. As in the equatorial IMF case discussed earlier, the distribution of perturbations is nonuniform and, as before, strongest on the flanks. The model-based perturbation field reproduces this result, which from the perspective of superposition models appears to be anomalous

3. Summary and Conclusions

The previous sections compare IMP 8 data-based and MHD model-based field and perturbation patterns. Before reviewing these results, we recall several points bearing on the comparability of the two, differently generated patterns. First, the MHD model is time dependent, and the patterns presented are snapshots, whereas the data-based patterns are 4-year averages. Second, the model-based patterns refer to conditions at exactly $x = -30\ R_E$, though the features seen in the maps do not change much in x. The data-based patterns, in contrast, are averages over $x = -25\ R_E$ to $-40\ R_E$, which is the range sampled by IMP 8. Third, the model has been run for a steady IMF that points straight duskward, northward, or southward for about 2 hours. The data-based results are averages over a variable IMF that can wander within 45° from straight duskward, dawnward, northward, or southward. Fourth, in the simulations after two hours, the tail is still evolving from the initial state. A better comparison therefore would be between the observations, which are in

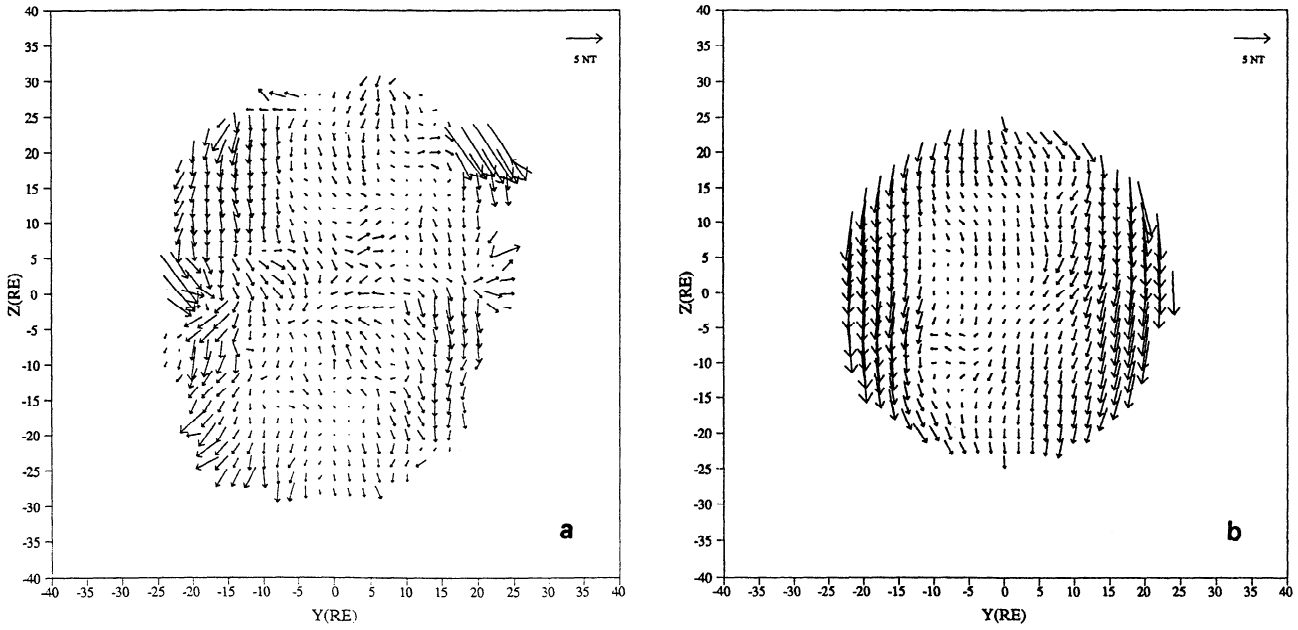

Figure 7. (a) IMP 8 north-south difference field vectors. (b) Fedder and Lyon MHD model north-south field difference vectors.

effect ensemble averages, and time averages over a longer model run. Finally, and probably most important, the history of the IMF in the solar wind plays an important role in the appearance of the detailed features in the model maps which might be averaged in the observed maps. These differences will degrade the degree of correspondence between the patterns.

Indeed, the model-based patterns exhibit some significant departures from the data-based patterns. In general their nodes are more complex, for example more elongated, multiple, and associated with spirals. The patterns common to both the simulations and the observations tend to be more exaggerated in the simulations. The lobe fields in the equatorial simulation are more magnetosheathlike than taillike. For southward IMF, lack of a B_y perturbation leaves the internodal component lines unapexed and the flaring component lines deficient in the horizontal type of component line. This last difference between the model and the data would be lessened, however, if the snapshots from the simulation were taken at a later time. Then lobe fields would be stronger and therefore less magnetosheathlike for both duskward IMF and southward IMF cases. That the model-based images show more structured nodes and more exaggerated effects might reflect shorter exposure times. The spatial averages, which are inherent in the IMP 8 data analysis, would tend to eliminate structures that have positions which are sensitive to the y component of the IMF or move as the magnetosphere evolves.

Beyond the differences between the simulations and the observations, the details of the agreements constitute a significant message regarding the operation on the global scale of MHD processes and the applicability of MHD codes. For duskward IMF they include the shearing of the internodal fields, the shifting of the nodes, and the twisting of the current sheet. For northward IMF they include the dominating circular dipole pattern. For southward IMF they include the dominating flaring component lines and the equatorially restricted dipolar component lines. Also probably most significant of all, in all cases they include the observed concentration of the perturbation fields to the equatorial flanks. This last agreement is particularly diagnostic because it is true only for the global MHD model; no other model known to us as yet predicts such a localization of the perturbations to the flanks. While the superposition model, discussed for example by *Cowley* [1973], gives the qualitative global geometry of Figure 1 and the sign of the perturbations in Figure 3, it also predicts uniform perturbations. Even regional MHD-based models such as *Voigt and Hilmer*'s [1987] magnetohydrostatic tail model and *Khurana*'s [1992] magnetospheric convection model, both of which predict the skewing of the component lines and the shifting of the nodes in the plasma sheet, do not explain the localization of the field perturbations for both equatorial and north-south directed IMFs. Global MHD models in which tail properties are controlled by dayside reconnection geometries evidently are needed to capture the tail's observed localization of IMF-related field perturbations.

Acknowledgements. This research was supported in part by the National Science Foundation under grant ATM 94-96139. The MHD modeling work was supported by NASA-SPTP and ONR.

The editor thanks S. W. H. Cowley and T. I. Pulkkinen for their assistance in evaluating this paper.

References

Cowley, S.W.H., A qualitative study of the reconnection between the Earth's magnetic field and an interplanetary field of arbitrary orientation, *Radio Sci., 8*, 903-913, 1973.

Fairfield, D.H., A statistical determination of the shape and position of the geomagnetic neutral sheet, *J. Geophys. Res., 85*, 775-780, 1980.

Fedder, J.A. and J.G. Lyon, The solar wind-magnetosphere-ionosphere current-voltage relationship,*Geophys. Res. Lett., 14*, 880-883,1987.

Fedder, J.A. and J.G. Lyon, The Earth's magnetosphere is 165 R_e long: or self consistent currents, convection, magnetospheric structure and processes for northward IMF, *J.Geophys. Res., 100*, 3623-3635, 1995.

Fedder, J.A., J.G. Lyon, S.P. Linker and C.M. Mobarry, Topological Structure of the magnetotail as a function of IMF direction, *J. Geophys. Res., 100*, 3613-3621, 1995.

Kaymaz, Z., G.L. Siscoe, N. A. Tsyganenko, and R. P. Lepping, Magnetotail views at 33 RE: IMP 8 magnetometer observations, *J. Geophys. Res., 99*, 8705-8730, 1994a.

Kaymaz, Z., G.L. Siscoe, J.G. Luhmann, R. P. Lepping, and C. T. Russell, Interplanetary magnetic field control of magnetotail magnetic field geometry: IMP 8 observations, *J. Geophys. Res., 99*, 11,113-11,126, 1994b.

Khurana, K.K., A model of magnetospheric convection in the presence of IMF B_y, publication # 3764, Inst. of Geophys. and Plant. Phys., Univ. of Calif., Los Angeles, 1992.

Tsurutani, B. T., D. E. Jones, R. P. Lepping, E. J. Smith, and D. G. Sibeck, The relationship between the IMF B_y and the distant tail (150-238 R_E) lobe and plasma sheet B_y fields, *Geophys. Res. Lett., 11*, 1082-1085, 1984.

Voigt, G.-H., and R. V. Hilmer, The influence of the IMF By component on the Earth's magneto-hydrostatic magnetotail, in *Magnetotail Physics*, edited by A. T. Lui, pp. 91-96, Johns Hopkins University Press, Baltimore, Maryland, 1987.

J. A. Fedder, Code 4790, Naval Research Laboratory, Washington, DC 20375. (e mail: fedder@ppd.nrl.navy,mil)

Z. Kaymaz, G. Siscoe Center for Space Physics, 725 Comonwealth Avenue, Boston University, Boston, MA 02215. (e mail: zerefsan@atmos.bu.edu; siscoe@buasta.bu.edu)

J. G. Luhmann, Space Science Laboratory, University of California, Berkeley, CA 94720. (e mail: jgluhmann@igpp.ucla.edu)

J. G. Lyon, Department of Physics and Astronomy, Dartmouth College, Hanover, NH 03755. (e mail: lyon@tinman.dartmouth.edu)

(Received November 1, 1994; revised February 13, 1995; accepted February 16, 1995.)